Study of cast-mono silicon solar cells with boron-doped PERL structure

WENJIA LI[a,*], ZHENJIAO WANG[c], LINA SU[a], JIAN REN[a], JIANBO SHAO[b]
[a]*Huaiyin Normal University, Huaian 223300, China*
[b]*Jiangnan University, Wuxi 214122, China*
[c]*Kingstone Semiconductor Co., Ltd, Shanghai 201203, China*

In this paper, passivated emitter and rear locally diffused (PERL) structure was employed on cast-mono silicon wafers to achieve high efficiency. Some critical fabrication parameters, such as sheet resistance, thickness of rear passivation stacks, laser pattern and sintering temperature, were discussed and optimized. The average and best efficiencies reached to 19.20% and 19.54% with 80Ω/□ sheet resistance (after oxidation), 240 nm rear SiO_2/SiN_x stacks, 1.2 mm laser pitch and 600℃ Al sintering. Afterwards, low temperature annealing in N_2 or air was performed on prepared cells. The efficiency of cells gained 0.18%abs after 150℃ annealing in N_2. Finally, light induced degradation (LID) was studied. PERL solar cells on cast-mono silicon degenerated 0.29%abs after illuminated with one sun for 200 minutes, which is much less than that of mono ones (1.04%abs) due to the comparatively low interstitial oxygen concentration in cast-mono wafers.

(Received June 26, 2017; accepted February 12, 2018)

Keywords: Solar cells, Cast-mono crystalline silicon, PERL, High efficiency, Light induced degradation

1. Introduction

In photovoltaic (PV) industry, many efforts have been made on cost reduction and efficiency improvement. This goal can be achieved through high quality but cost-effective material and cell structure optimization. Both mono crystalline and multi-crystalline (mc) silicon wafers are the dominating substrate materials for traditional solar cells. Recent years, manufacturers are partial to mc silicon substrate due to their relatively low cost as compared to mono crystalline material. However, mc silicon is not the most appropriate material for solar cell fabrication because the grain boundaries, high density of dislocations and the metallic impurity precipitate which can extremely decrease minority carrier lifetime. Therefore, more and more investigations have being concentrated on a more promising material—cast-mono crystalline silicon, which can be considered as an ideal substrate for silicon solar cells: square, single crystalline, of low structural defect density and with low fabrication cost [1].

In 2006, BP Solar first began growing ingot, which was called Mono 2, in a directional solidification system (DSS) furnace by utilizing a mono crystalline seed layer. This is a proprietary growth uncleation method for casting mono silicon bricks. As Mono 2 wafers are less expensive than the CZ wafers and have fewer defects than mc wafers, they are attracting particular attention. From then on, many efforts have been made on cast-mono crystalline silicon solar cells. Cells with various high efficiency structures and technologies such as metal wrap through (MWT) cells [2], passivated emitter and rear contact (PERC) cells [3], i-PERC cells [4], laser firing contact (LFC) cells [5] and n-type heterojunction cells [6] that applied on cast-mono substrate have been reported.

PERL structure was always investigated on mono crystalline silicon wafers [7-9]. Wang [10] has reported that cells based on PERL structure has accomplished a 20.3% efficiency for standard commercial p-type single crystalline silicon wafers with a 40.9 mA/cm^2 current density. However, PERL cell fabricated on cast-mono substrate was rarely reported. In this work, we have demonstrated the effect of parameters of key processes, such as sheet resistance (R_{sh}), thickness of rear passivation layer (SiO_2/SiN_x), rear laser pattern and sintering temperature of rear contact on cast-mono PERL cells. Besides, as finished PERL cells made on mono substrate gained a 0.44% efficiency boost after 15min, 150°C annealing in N_2 [11], this low temperature process was also applied on the prepared cast-mono cells. It is found that the cast-mono PERL cells showed a little efficiency enhancement (0.18%abs). Moreover, as light induced degradation (LID) seriously limited cells performance, LID on both mono PERL cells and cast-mono PERL cells was studied. It has been found that cast-mono PERL cells which benefit from low bulk oxygen concentration deteriorated much less than mono PERL cells after 200 minutes illumination.

2. Experimental

The PERL cells were fabricated on 125mm×125mm,

180μm, p-type cast-mono crystalline silicon wafers with bulk resistivity in 1-3Ω·cm range. The following processes were undertaken in the preparation of substrates: (1) alkaline texturing, (2) single-side acid polishing, (3) SPM cleaning and p-n junction thermal diffusion, (4) wet rear etch and edge isolation, (5) SPM cleaning and thermal oxidation (10nm) on both sides, (6) double-sided SiN_x:H (front: 80nm, rear: 180nm or 240nm) by in-line PECVD, (7) 800°C firing in in-line furnace to enhance the passivation effect, (8) liquid boron source spinning and baking, (9) laser ablation and doping with pitch of lines being 1.0mm (or pitch of dots being 0.5mm), (10) 400°C forming gas annealing in a chamber, (11) rear Al sputtering and 570°C (or 600°C) sintering, (12) front laser doping and light-induced plating (LIP).

The samples were divided into four pairs of groups according to four variables: the sheet resistance (R_{sh}) after oxidation (group A 80Ω/□ and group B 120Ω/□), the rear SiN_x thickness (group C 180nm and group D 240nm), the rear laser pattern (group E line and group F dot) and the Al sintering temperature (group G 570°C and group H 600°C). The finished cells were measured under standard illumination conditions (AM1.5G, 25°C) to get J-V parameters. Reflectivity, internal quantum efficiency (IQE) and SEM images were displayed. The suitable R_{sh}, rear SiN_x thickness, rear laser pattern and sintering temperature were chosen after analyzing the results.

Subsequently, the prepared cells fabricated with optimized processes were treated by 15min, 150°C annealing. The samples in group (1) were immersed in N_2 while cells in group (2) were exposed in air. The electrical properties of these cells were measured under standard illumination conditions (AM 1.5G, 25°C).

After that, a batch of finished cast-mono PERL cells (group i) and some mono PERL cells (group ii) were illuminated by halogen lamps with 1000 W/m^2 (one sun) for 200 minutes. Cell parameters were measured before and after each degradation step. The measurement was performed at 25°C as soon as the samples were removed from the illumination. Fig. 1 shows the process flow of the whole experiment.

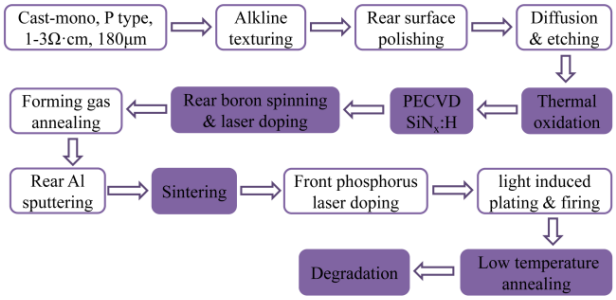

Fig. 1. The process flow of the whole experiment

3. Results and discussion

3.1. Optimization of fabrication processes for cast-mono PERL cells

3.1.1. Sheet resistance

As high R_{sh} is conducive to light absorption in short-wave band and recombination reduction, mono PERL cells with front selective emitter fabricated by LIP usually prepared with high R_{sh} (120Ω/□ after oxidation) [11-12]. In this section, effect of R_{sh} on PERL cells made on cast-mono silicon was measured.

Table 1 lists the electric properties of cast-mono PERL cells with different sheet resistances. Cells with 80Ω/□ R_{sh} show lower J_{sc} and V_{oc} but higher FF and Eff compared with cells with 120Ω/□ R_{sh}. Higher J_{sc} and V_{oc} of group B is benefit from higher R_{sh} (120Ω/□). The enhanced light absorption in short-wave band could improve J_{sc}, while the decreased p-n junction recombination leads to a higher V_{oc}. However, light diffused cells also suffer from high series resistance (R_s), which contributes to an inferior FF, as shown in group B. As a result, 80Ω/□ R_{sh} was selected based on a tradeoff among J_{sc}, V_{oc}, FF and Eff.

Table 1. Electric properties of cast-mono PERL cells with different sheet resistances after oxidation

Group	R_{sh}(Ω/□)	V_{oc}(mV)	J_{sc}(mA/cm^2)	FF(%)	Eff(%)	R_s(mΩ)
A	80	643.5	38.74	76.21	19.00	3.9
B	120	646.4	38.85	75.22	18.89	4.1

3.1.2. Rear SiN_x thickness

Table 2, which describes properties of cells with different rear SiN_x thickness, demonstrates that 240 nm is the better rear SiN_x thickness for cast-mono PERL cells. Although group D shows a lower J_{sc} and V_{oc}, it presents a superior FF and Eff. As the sole difference between group C and D is rear SiN_x thickness, the reflectance of cells in each group was collected to reveal the reasons of results listed in Table 2.

Table 2. Electric properties of cast-mono PERL cells with different rear SiN_x thickness

Group	Rear SiN_x thickness(nm)	V_{oc}(mV)	J_{sc}(mA/cm^2)	FF(%)	Eff(%)	R_s(mΩ)
C	180	652.6	38.89	74.71	18.96	4.4
D	240	650.7	38.78	75.65	19.09	4.1

Fig. 2 indicates the rear surface reflectance (internal reflection) of cells in group C and D. As depicted in Fig. 2, the reflectance at 1200 nm of group C and D is 49.2% and 46.5%, respectively. It is suggested that thickness of SiN_x could effect the reflectance, especially at long-wave band. Higher reflectance could reflect more light into the active regions by SiN_x/sputtered Al reflector for further absorption, instead of escaping from the rear surface or being absorbed during internal reflection [11]. This would increase carrier collection at infrared wavelength and achieve a higher J_{sc}. That is why J_{sc} of group C is a little higher than that of group D.

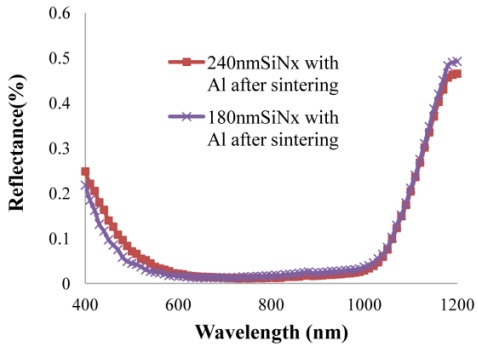

Fig. 2. Rear surface reflectance of cells in group C (180 nm rear SiN_x) and D (240nm rear SiN_x) after Al sintering

V_{oc} is given by:

$$V_{oc} = \frac{kT}{q} \ln\left(\frac{J_{sc}}{J_o} + 1\right) \quad (1)$$

where k is Boltzmann's constant, q is electronic charge, T is the absolute temperature and J_o is saturation current density. With the increase of J_{sc}, V_{oc} also gets promoted.

Comparatively, cells with 240 nm SiN_x shows preferable FF. This is ascribe to the reflectance of SiN_x on doping laser. The reflectance of 180 nm and 240 nm SiN_x layer on 355 nm doping laser employed in this experiment is 32% and 27%, respectively. The higher the reflectance on doping laser is, the less the heat absorbs by silicon. With less thermal radiation, laser doped boron concentration of group C is not as much as group D. This directly leads to a higher R_s and a lower FF of group C compared with group D. Finally, the loss of FF exceeds the gain of J_{sc} and V_{oc} for group C. Therefore 240 nm rear SiN_x is chosen in order to balance FF with J_{sc} and V_{oc}.

3.1.3. Rear laser pattern

Table 3 summarizes average electric properties of cast-mono PERL cells with different rear laser pattern. J_{sc} and V_{oc} of group E is inferior to that of group F, while FF and Eff show a contrary result. Fig. 3 demonstrated the SEM images of rear contact. As can be seen in Fig. 3, the width of line is 28μm while the radius of dot is 33.2 μm. The contact area is given by:

$$f_{line} = \frac{d}{p} \times 100\% \quad (2)$$

$$f_{dot} = \frac{\pi r^2}{p^2} \times 100\% \quad (3)$$

where d is width of line, r is radius of dot, p is pitch between lines or dots. The calculated contact area is 2.33% and 1.39% for group E and F, respectively. It is reported that [13] when the contact area proportion is more than 1%, not only the optical properties of the rear surface would be effected, but also the recombination centers would be increased which exacerbates the rear surface recombination velocity (SRV). Moreover, this change is nonlinear. The rear surface reflectance (internal reflection) of group E and F were collected in Fig. 4. As shown in Fig. 4, the reflectance at 1200 nm of group F is 46.9% which is a little higher than that of group E 43.6%. This result is responsible for the higher J_{sc} of group F. Similarly, smaller contact area implies larger passivated area proportion, which is beneficial to reduce rear SRV. This results in a preferable V_{oc} of group F.

Nevertheless, smaller contact area also means bigger lateral resistance which is one part of R_s. As can be seen in Table 3, the R_s of group F is 0.7 mΩ higher than that of group E. Thus group E demonstrates a much better FF. Finally, as the improvement of FF outweighs the promotion of J_{sc} and V_{oc}, rear laser pattern of line with 1.2 mm pitch is selected.

Table 3. Electric properties of cast-mono PERL cells with different rear laser pattern

Group	Rear laser pattern	Contact Area(%)	V_{oc}(mV)	J_{sc}(mA/cm^2)	FF(%)	Eff(%)	R_s(mΩ)
E	Line with 1.2mm pitch	2.33	643.5	38.74	76.21	19.00	3.9
F	Dot with 0.5mm pitch	1.39	646.7	38.95	73.72	18.57	4.6

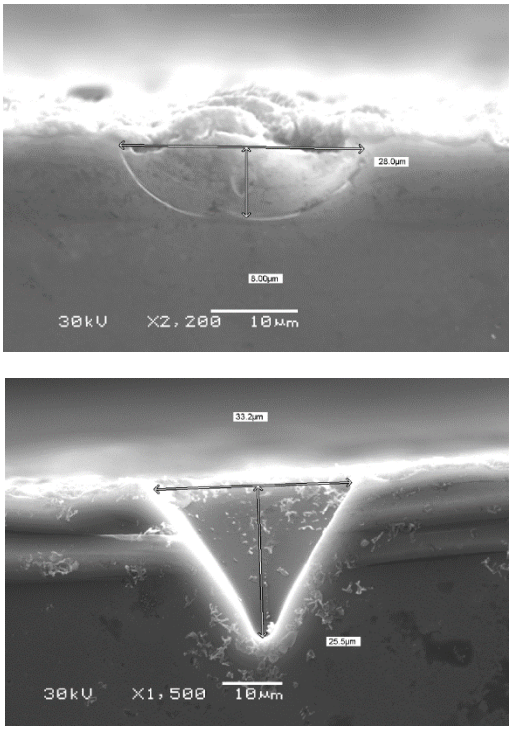

Fig. 3. Rear contact SEM images of line and dot

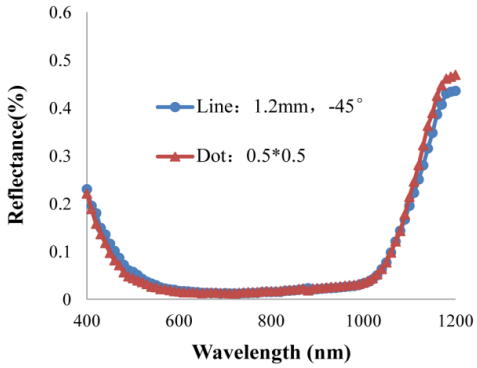

Fig. 4. Rear surface reflectance of cells in group E (rear pattern is line with 1.2mm pitch) and F (rear pattern is dot with 0.5mm pitch)

3.1.4. Al sintering temperature

In order to form a boron-back surface field (B-BSF), Al sintering temperature could not be too high [11]. Therefore 570°C and 600°C was studied in this experiment. Table 4 exhibits the electric properties of cast-mono PERL cells with different Al sintering temperature. 570°C sintered cells demonstrate higher J_{sc} and V_{oc}, while 600°C sintered cells show superior FF and Eff.

Table 4. Electric properties of cast-mono PERL cells with different Al sintering temperature

Group	Rear laser pattern(°C)	Contact Area(%)	V_{oc}(mV)	J_{sc}(mA/cm^2)	FF(%)	Eff(%)	R_s(mΩ)
G	570	1.49	655.3	38. 97	74.55	19.04	4.4
H	600	2.33	650.7	38. 78	75.65	19.09	4.1

The rear contact SEM images of 570°C and 600°C sintering are displayed in Fig. 5. Calculated by equation (2), the rear contact proportion of group G and H is 1.49% and 2.33% respectively. Thus the optical properties of the rear surface would be different. Fig. 6 depicted the rear surface reflectance (internal reflection) of cells in group G and H. Higher sintering temperature creates a larger Si/Al interface. Correspondingly, the effective area of Si/passivation stacks/Al interface which act as a more functional rear reflector would be decreased. Consequently, the reflectance at 1200 nm of group G (46.6%) is a little higher than that of group H (42.6%) as shown in Fig. 6. Although 600°C sintering is conducive to form a heavier B-BSF which is helpful to enhance J_{sc}, the improvement brought by rear reflector overrides the increase induced by B-BSF. At last, J_{sc} of group G is 0.19mA/cm^2 higher than that of group H.

The contact area proportion also contributes to the results of V_{oc} and FF in group G and H which is similar with that in group E and F. Considering the efficiency of each group, 600°C is decided to be the sintering temperature.

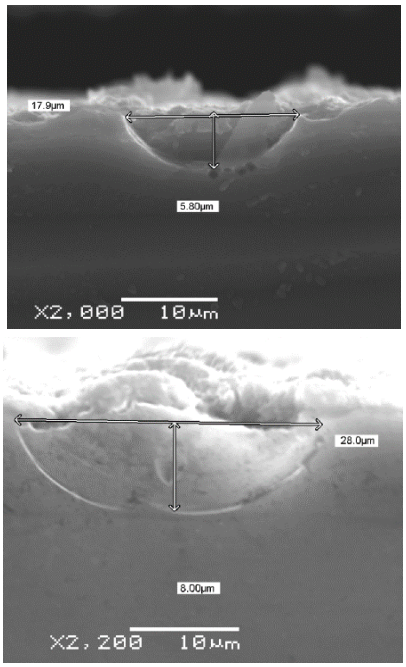

Fig. 5. Rear contact SEM images of 570°C and 600°C Al sintering

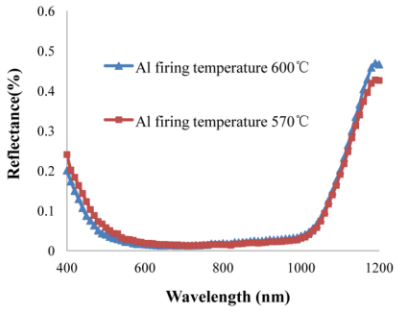

Fig. 6. Rear surface reflectance of cells in group G (570℃ Al sintering) and H (600℃ Al sintering)

After optimize some essential processes, electric properties of cast-mono PERL cells are listed in Table 5. An 19.20% average efficiency was achieved. J_{sc} of the best cell (19.54% efficiency) reached 39.28 mA/cm^2 which is equivalent to mono PERL cells' level [11].

Table 5. Electric properties of cast-mono PERL cells with optimized processes

	V_{oc}(mV)	J_{sc}(mA/cm^2)	FF(%)	Eff(%)	R_s(mΩ)
Best	654.1	39.28	76.05	19.54	4.0
Average	650.7	38.99	75.69	19.20	4.2

3.2. Low temperature annealing

Low temperature annealing has already been employed to improve the performance of organic solar cells [14-16], thin film solar cells [17] and mono PERL cells [11]. In this section, the effect of low temperature annealing on finished cast-mono PERL cells was studied.

Table 6 demonstrates the electric properties of cast-mono PERL cells before and after 15min, 150℃ annealing in certain atmospheres: 100%N_2 and air (78%N_2+21%O_2). Although not so obvious, the efficiency shows a 0.18% increase after annealing in N_2 and a 0.11% decrease after treated in air. For group (1), the raise of cells' performance is primarily attributed to the improvement of FF (from 75.69% to 75.99%) and J_{sc} (from 38.99 to 39.18 mA/cm^2). For group (2), degraded J_{sc} (from 38.99 to 38.88 mA/cm^2) and FF (from 75.69% to 75.50%) are responsible for the deterioration of efficiency. The influence of V_{oc} to efficiency is little in both group (1) and (2).

Boron atoms widely exist in silicon bulk and doped area. It is believed that part of boron atoms were passivated by oxygen and become BO_i pairs which decrease the boron atoms' activity. The increase of active boron concentration in silicon bulk contributes to a drop of lateral resistance while the growth of active boron concentration in heavily doped area leads to a decrease of contact resistance, and vice versa. Decline of lateral resistance and contact resistance jointly decrease the R_s and hence increase the FF. Moreover, the higher the active boron concentration in doped area is, the better the metal-semiconductor contact forms. This is beneficial to improve J_{sc}. In this case, as 15min 150℃ N_2 thermal annealing could convert the BO_i pairs into electrically active boron atoms, the R_s can then be diminished while both FF and J_{sc} get enhanced. On the contrary, air provides sufficient oxygen which would passivate active boron, so that thermal treatment in air could increase the BO_i pairs and even cause the counterproductive effect on FF and J_{sc}.

Table 6. Electric properties of cast-mono PERL cells after 15min, 150℃ annealing

Group	Atmosphere	V_{oc}(mV)	J_{sc}(mA/cm^2)	FF(%)	Eff(%)	R_s(mΩ)
Untreated	n/a	650.7	38.99	75.69	19.20	4.2
(1)	100%N_2	650.9	39.18	75.99	19.38	4.1
(2)	air(78%N_2+21%O_2)	650.3	38.88	75.50	19.09	4.3

For thorough testify the mechanism, Table 7 summarized the electric data of low temperature annealing on mono PERL cells and mono PERC cells in our previous work [11]. As can be seen from Table 7, mono PERL cells show a 0.44%abs efficiency boost after annealing in N_2. The enhancement of mono PERL cells is because of the rise of J_{sc} (from 39.28 mA/cm^2 to 39.37 mA/cm^2), V_{oc} (from 662.5mV to 666.3mV), and FF (from 74.82% to 75.91%)) which is caused by the decreased R_s (from 4.7mΩ to 4.2mΩ). By contrast, cast-mono PERL cells and mono PERC cells gain a 0.18% and 0.07% efficiency improvement, respectively.

On one hand, as rear surface of PERL cell is locally diffused by boron, the boron concentration of cells in groups I andII (doped area [B]=4.3×10^{20}cm^{-3}) is much higher than that of PERC cells in group III which have not been laser doped. On the other hand, the interstitial oxygen content in cast-mono wafers (2.0Ω cm, [O_i]=2.2×10^{17}cm^{-3}) is much lower than that of mono wafers (1.6Ω cm, [O_i]=1.0×10^{18}cm^{-3}). Obviously, both boron and oxygen content of mono PERL cells in group II are high, which is easily to form BO_i pairs. Therefore cells properties of

group II obtain an apparent boost after thermal annealing in anaerobic atmosphere which is the boron activation process. Comparatively, group I with lower oxygen content and group III which is lack of boron atoms could form less BO_i pairs compared with group II. Thus the thermal process has not taken noticeable effect on cells of these two groups. Consequently, it is deduced that the BO_i pair mechanism is applicable.

Table 7. Electric properties of different cells before and after 15min, 150°C annealing in N_2

Group		O content	B content		V_{oc}(mV)	J_{sc}(mA/cm^2)	FF(%)	Eff(%)	R_s(mΩ)
I	Cast-mono PERL	low	high	Before anneal	650.7	38.99	75.69	19.2	4.2
				After anneal	650.9	39.18	75.99	19.38	4.1
II	Mono PERL	high	high	Before anneal	662.5	39.28	74.82	19.47	4.7
				After anneal	666.3	39.37	75.91	19.91	4.2
III	Mono PERC	high	low	Before anneal	661.1	38.78	76.00	19.48	4.1
				After anneal	661.8	38.84	76.07	19.55	4.1

3.3. LID of cast-mono silicon solar cell

Fischer and Pschunder [18] have found that boron-doped mono silicon solar cells inevitably suffer severe efficiency degradation under long time sunlight illumination. Schmidt [19] has ascribed this low light-degraded efficiency to BO_i pairs. Furthermore, decomposition and recombination of Fe_iB_s pair was induced to explain LID because Fe_i and Fe_iB_s pair show markedly different recombination properties [20]. For mono cells with high oxygen content, BO_i pair is the dominant degradation mechanism, while Fe_i leads the deteriorating of mc-silicon cells [21]. But it is well known that mc-silicon solar cells are much more resistance to LID than mono silicon solar cells. Schmidt's study [19] implied that LID can be suppressed by reducing either boron or oxygen concentration in silicon wafers. Current researches [1] has found that the LID effect on cast-mono cells which are fabricated by traditional screen printing technology is minimized due to the comparatively low interstitial oxygen concentration. In this sense, cast-mono PERL cell is supposed to inherit the same merits.

Table 8 summarized the electric properties of mono and cast-mono PERL cells before and after 200 minutes, 1000 W/m^2 (one sun) illumination. Tendency of efficiency, V_{oc}, J_{sc}, FF and R_s of mono and cast-mono PERL silicon solar cells during 200 minutes illumination are presented in Fig. 7. Data in Table 8 and Fig. 7 jointly demonstrate that both mono and cast-mono PERL cells show the downward trend. The efficiency dropped by 0.29%abs and 1.04%abs for cast-mono and mono PERL cells, respectively. The attenuation is more serious on mono PERL solar cells. For cast-mono PERL cells, the primary factor of attenuation is FF, while both V_{oc} and FF dominate the degradation of mono PERL cells.

Table 8. Electric properties of mono and cast-mono PERL cells before and after 200 minutes, 1000 W/m^2 (one sun) illumination

		V_{oc}(mV)	J_{sc}(mA/cm^2)	FF(%)	Eff(%)	R_s(mΩ)
Cast-mono PERL	before	657.8	38.78	75.45	19.25	4.2
	after	657.4	38.65	74.62	18.96	4.4
Mono PERL	before	658.6	38.77	78.17	19.96	3.9
	after	647.4	38.60	75.69	18.92	4.8

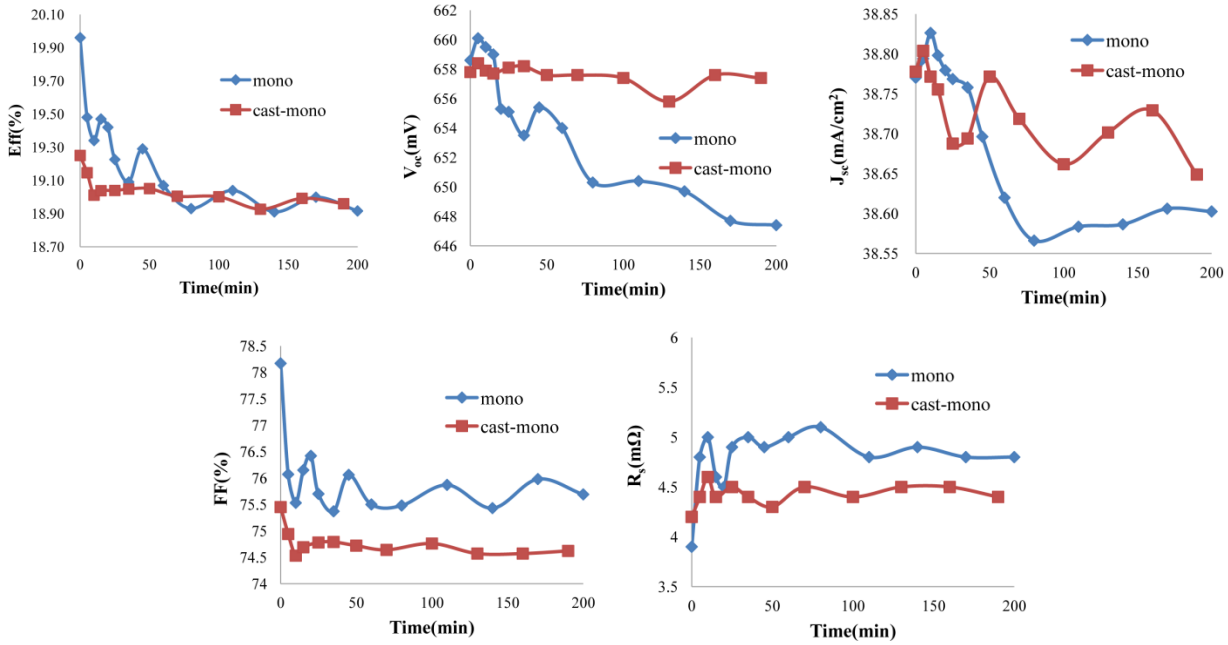

Fig. 7. Variation trend of electric properties (Eff, V_{oc}, J_{sc}, FF, R_s) of mono and cast-mono PERL cells illuminated by halogen lamps with 1000 W/m^2 (one sun) for 200 minutes

As Fe_i and BO_i defects are two main attenuation factors of solar cells, it is important to figure out which mechanism dominates the degradation of mono and cast-mono cells. There is a method to distinguish Fe_i degradation mechanism from BO_i pair: degradation induced by Fe_i can be recovered in a couple of hours in the dark at room temperature [20], while cells cannot get rid of BO_i defects without thermal treatment above 200°C [18]. Therefore, after 20 hours in dark at room temperature the illuminated cells were tested again. After that, they underwent 200°C thermal treatment. The results are listed in Table 9.

Table 9. Electric properties of mono and cast-mono PERL cells after illumination, 20 hours in dark and 200°C thermal treatment

	Illumination	20 hours in dark	200°C treatment
cast-mono cell	18.96%	19.15%	19.22%
mono cell	18.92%	19.20%	19.87%

The mono PERL cells show 0.28%abs and 0.67%abs increase in efficiency after 20 hours in dark and 200°C thermal treatment respectively. It appears to be that although Fe_i defects lead to LID of mono PERL cells, the main LID mechanism is BO_i pair activated by illumination. For cast-mono PERL cells, 0.19%abs efficiency recovery is observed after cells were kept in dark for 20 hours at room temperature. On the contrary, the efficiency barely promotes 0.07%abs after 200°C thermal treatment. It is deduced that Fe_i defects dominate the degradation of cast-mono PERL cells instead of BO_i pair. These results suggest that the weaker LID of cast-mono PERL cells is attributed to an inherently reduced oxygen content (2.0Ω cm, $[O_i]=2.2\times10^{17}cm^{-3}$) of the cast-mono Si wafers, which is almost one order of magnitude less than that of mono Si wafers (1.6Ω cm, $[O_i]=1.0\times10^{18}cm^{-3}$). Finally, with low oxygen content, cast-mono PERL cells are much more stable than mono PERL cells.

After illumination, the efficiency gap between the cast-mono and mono PERL cells is very little. The performance of cast-mono PERL cells is even better than that of mono ones. This advantage of cast-mono PERL cells on stability makes it more cost-effective to be applied in industry.

4. Conclusion

In this paper, cast-mono cells with boron-doped PERL structure were studied.

(1) Some critical fabrication parameters, such as sheet resistance after oxidation, thickness of rear passivation stacks, laser pattern and sintering temperature, were discussed and optimized. After balance FF with J_{sc} and V_{oc}, average and best efficiencies reached to 19.20% and 19.54% with 80Ω/□ sheet resistance (after oxidation), 240nm rear SiO_2/SiN_x stacks, 1.2mm laser pitch and 600°C Al sintering.

(2) 150°C low temperature annealing in N_2 was employed on prepared cells. Cells efficiency gained 0.18%abs after treated in N_2 at 150°C. As this low temperature annealing in N_2 could convert the BO_i pairs into electrically active boron atoms, the R_s can then be diminished while both FF and J_{sc} get enhanced.

(3) Light induced degradation was studied. Cast-mono PERL cells degenerated 0.29%abs after illuminated with one sun for 200 minutes, which is much less than that of mono PERL cells (1.04%abs) due to the comparatively low interstitial oxygen concentration in cast-mono wafers. This superior stability makes cast-mono PERL cells possible to be a cost-effective production.

Acknowledgments

The authors would like to thank Yongfei Jiang of Suntech Co., Ltd for support in experiments and discussion. The authors gratefully acknowledge the financial support from the Project supported by the Natural Science Foundation of the Higher Education Institutions of Jiangsu Province (Grant No. 17KJB535001).

References

[1] X. Gu, X. Yun, K. Guo, L. Chen, D. Wang, D. Yang, Sol. Energ. Mat. Sol. C. **101**, 95 (2012).
[2] W. Yin, X. Wang, F. Zhang, L. Zhang, IEEE J. Photovolt. **3**, 697 (2013).
[3] B. Sun, J. Sheng, S. Yuan, C. Zhang, Z. Feng, Q. Huang, Proc. 38th IEEE Photovolt. Specialists Conf. Austin, Texas, 2012, p. 1125.
[4] V. Prajapati, E. Cornagliotti, R. Russell, J. Fernandez, R. F. Clark, N. Stoddard, P. Choulat, J. John, Proc. 24th Proc. 27-th EU PVSEC, Frankfurt, Germany, 2009, p. 1171.
[5] C. Schwab, J. Haunschild, M. Graf, C. Wufka, A. Wolf, D. Biro, R. Preu, Energy Proc. **38**, 611 (2013).
[6] F. Jay, D. Muñoz, T. Desrues, E. Pihan, V. Amaral de Oliveira, N. Enjalbert, A. Jouini, Sol. Energ. Mat. Sol. C **130**, 690 (2014).
[7] A. Cacciato, F. Duerinckx, K. Baert, M. Moors, T. Caremans, G Leys, K. De Keersmaecker, J. Szlufcik, Sol. Energ. Mat. Sol. C **113**, 153 (2013).
[8] H. Li, S. Wenham, Z. Shi, Sol. Energ. Mat. Sol. C. **117**, 41 (2013).
[9] E. Cornagliotti, A. Uruena, B. Hallam, L. Tous, R. Russell, F. Duerinckx, J. Szlufcik, Sol. Energ. Mat. Sol. C **138**, 72 (2015).
[10] Z. Wang, P. Han, H. Lu, H. Qian, L. Chen, Q. Meng, N. Tang, F. Gao, Y. Jiang, J. Wu, W. Wu, H. Zhu, J. Ji, Z. Shi, A. Suginanto, L. Mai, B. Hallam, S. Wenham, Prog. Photovoltaics **20**, 260 (2012).
[11] W. Li, Z. Wang, P. Han, H. Lu, J. Yang, Y. Guo, Z. Shi, G Li, Appl. Surf. Sci. **311**, 344 (2014).
[12] W. Li, Z. Wang, P. Han, Y. Wang, Z. Shi, G Li, Optoelectron. Adv. Mat. **10**(3-4), 159 (2016).
[13] D. Kray, M. Hermle, S. Glunz, Prog. Photovoltaics **16**(1), 1 (2008).
[14] B. Ray, P. Nair, M. Alam, Sol. Energ. Mat. Sol. C **95**, 3287 (2011).
[15] C. Shih, K. Hung, H. Wu, S. Fu, H. Chen, C. Hsiao, Org. Electron. **13**, 373 (2012).
[16] I. Kim, G Jabbour, Synthetic Met. **162**, 102 (2012).
[17] Y. Chung, D. Cho, N. Park, K. Lee, J. Kim, Curr. Appl. Phys. **11**(1), S65 (2011).
[18] H. Fisher, W. Pschunder, Proc. 10th IEEE Photovolt. Specialists Conf., Palo Alto, California, 1973, p. 404.
[19] J. Schmidt, A. Aberle, R. Hezel, Proc. 26th IEEE Photovolt. Specialists Conf., Anaheim, California, 1997, p. 13.
[20] J. Schmidt, Prog. Photovoltaics **13**(4), 325 (2005).
[21] D. Macdonald, L. Geerligs, A. Azzizi, J. Appl. Phys. **95**(3), 1021 (2004).

*Corresponding author: liwenjia0921@foxmail.com